Journal of Materials Chemistry A

Accepted Manuscript

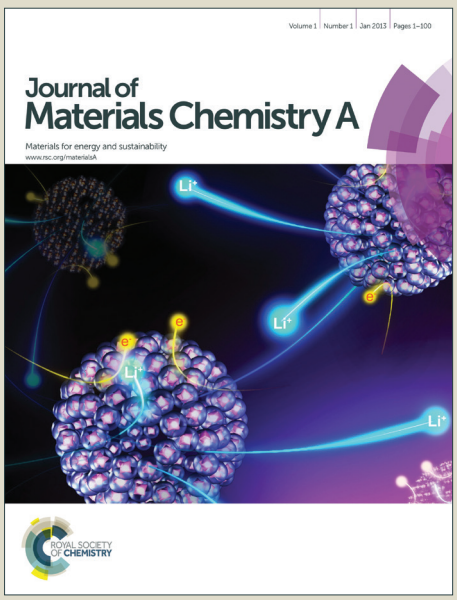

ROYAL SOCIETY OF CHEMISTRY

www.rsc.org/materialsA

Amorphous monodispersed hard carbon micro-spherules derived from biomass as a high performance negative electrode material for sodium-ion batteries

Yunming Li[‡], Shuyin Xu[‡], Xiaoyan Wu, Juezhi Yu, Yuesheng Wang, Yong-Sheng Hu*, Hong Li, Liquan Chen, Xuejie Huang

Keywords: Energy storage; Sodium-ion batteries; Anode; Hard carbon.

This study reports a monodispersed hard carbon micro-spherules with high energy density, high initial Coulombic efficiency and excellent cycle performance.

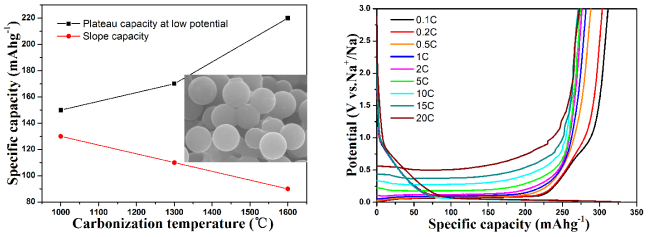

Amorphous monodispersed hard carbon micro-spherules derived from biomass as a high performance negative electrode material for sodium-ion batteries

By Yunming Li[‡], Shuyin Xu[‡], Xiaoyan Wu, Juezhi Yu, Yuesheng Wang, Yong-Sheng Hu, Hong Li, Liquan Chen, Xuejie Huang*

Prof. Y.-S. Hu, Y. M. Li, S. Y. Xu, X. Y. Wu, J. Z. Yu, Y. S. Wang, Prof. H. Li, Prof. L. Q. Chen, Prof. X. J. Huang
Beijing National Laboratory for Condensed Matter Physics, Institute of Physics, Chinese Academy of Sciences, Beijing 100190, China
E-mail: yshu@aphy.iphy.ac.cn

‡ Y. M. Li and S.Y. Xu contributed equally to this work.

Keywords: Energy storage; Sodium-ion batteries; Anode; Hard carbon.

Abstract

Sodium-ion batteries (SIBs) are a promising commercial alternative to lithium-ion batteries (LIBs) for large-scale and low-cost electrical energy storage applications in the near future. However, the absence of appropriate negative electrode material hinders their development. In this contribution, we synthesized a monodispersed hard carbon spherules (HCS) from an abundant biomass of sucrose, and investigated the influence of carbonized temperature on micro-structure and electrochemical performance for the first time. The initial Coulombic efficiency of the HCS is enhanced to 83% by coating a soft carbon on its surface through the pyrolysis of toluene. Interestingly, the plateau capacity at the low potential region increases with the increase of carbonization temperature. The HCS carbonized at 1600°C shows the highest plateau capacity (220 mAh g^{-1}) and excellent cycling performance with a capacity retention of 93% after 100 cycles. When coupled with air-stable P2-$Na_{2/3}Ni_{1/3}Mn_{2/3}O_2$ positive electrode, the full cell exhibits a high initial Coulombic efficiency of 76%, an average operating voltage of 3.5 V and excellent cycling performance. The theoretical energy density of this system is estimated to be 200 Wh/kg. These desired promising properties are believed to be close to the level of practical application.

Introduction

Lithium based batteries have been successfully developed as a power source for portable electronics due to their outstanding energy and power density since their first commercialization in 1991.[1] They are also now a promising alternative source for electric vehicles.[2,3] However, limited lithium source may hinder their application in the large-scale energy storage for smart grid and solar/wind energy.[4-6]

Sodium is the second alkali metal next to lithium and has similar physical and chemical properties.[7] In addition, sodium in principle unlimitedly distributes in the ocean,[8] therefore the low cost of sodium salts would pave the way for large-scale application. Sodium-ion batteries have attracted extensive attentions as a kind of energy storage technology in recent years.[9] So far there have been some positive electrode materials for SIBs,[10-14] while the major obstacle in realizing SIBs is the absence of suitable negative electrodes. Probably due to the unique feature of large and highly ionized Na^+ ion, graphite material, which has been widely used as a negative electrode material for LIBs, shows poor sodium storage performance in SIBs.[15,16] The proposed negative electrode materials mainly include amorphous carbon materials, alloys, Ti-based oxides and organic compounds[17]. Na alloy negative electrode materials have high reversible capacities. Nanocomposites of Sb/C[18] and Sn/C[19] exhibit a high capacity of 610 mAh g^{-1} and 295 mAh g^{-1}, respectively. Recently, a composite electrode of SnSb/C was reported to deliver a large reversible capacity of 540 mAh g^{-1} with 80% capacity retention over 50 cycles.[20] The main problem of alloys lies in the structure destruction caused by the large volume expansion in the reaction with Na.[21] Ti-based oxides mainly include $Na_2Ti_3O_7$,[22] $Li_4Ti_5O_{12}$[23,24] and $Na_{0.66}[Li_{0.22}Ti_{0.78}]O_2$,[25] but the storage capacity is not high. Organic compounds such as disodium terephthalate ($Na_2C_8H_4O_4$) can deliver a large reversible capacity with good capacity retention in SIBs.[26,27] Nevertheless, low initial Coulombic efficiency and insufficient electronic conductivity limit the application of organic compounds. Recently, expanded graphite was fabricated as anode material for SIBs, but the first Coulombic efficiency is only 49.53%.[28] Hard carbon is likely to be the most promising alternative to graphite electrodes[29-31] because of relatively high capacity, natural abundance and renewability. Reversible Na extraction/insertion in hard-carbon was first reported by Stevens and Dahn in 2000.[32] The hard-carbon electrodes delivered ca. 300 mAh g^{-1} of reversible capacity, but the cycle performance is insufficient. Komaba *et al* significantly improved the cycle performance of hard carbon electrode by optimizing electrolyte, and fabricated hard-carbon/$NaNi_{0.5}Mn_{0.5}O_2$ cells.[33] However, the hard carbon electrode only shows a low capacity of 250 mAh g^{-1}, the hard-carbon/$NaNi_{0.5}Mn_{0.5}O_2$ full cells also only exhibit a capacity of 200 mAh g^{-1} with moderate cycling performance. Up to now, numerous carbon materials with various morphologies have been proposed for SIBs,[34-37] but their initial Coulombic efficiency and cyclic stability cannot satisfy the requirement of practical application.

Sucrose is an abundant and renewable raw material from biomass for producing hard carbon. Here we prepared hard carbon spherules with perfect spherical

morphology and smooth surface through the hydrothermal process and pyrolysis of sucrose. The initial Coulombic efficiency can be further improved by coating a soft carbon on its surface from pyrolyzing toluene. It is also very interesting to find that a higher carbonization temperature leads to a higher sodium storage capacity. In particular, the plateau capacity at the low potential region significantly increases, which is desirable for achieving a higher energy density in full cell.

Experimental

Materials synthesis

HCS was prepared by the pyrolysis of sucrose in two steps, namely dewatering at low temperature and carbonization at high temperature. In the first step, 1 M sugar solution was filled in stainless steel autoclave with a fill rate of 90%, and treated for hydrothermal at 190°C to get black powder according to previous work.[38-40] In the second step, the obtained black powder was carbonized for 2 hours in a tube furnace under Ar and toluene flow,then all samples were naturally cooled to room temperature. The carbonization temperatures were 1000°C, 1300°C and 1600°C, respectively.

Materials characterization

The structure was characterized by an X'Pert Pro MPD X-ray diffractometer (XRD) (Philips, Netherlands) using Cu-Kα radiation (1.5405 Å) and Raman spectra (JY-HR 800). The morphologies of the samples were investigated with a scanning electron microscope (SEM) (Hitachi S-4800). Nitrogen adsorption and desorption isotherms were determined by nitrogen physisorption on a Micrometritics ASAP 2020 analyzer.

Electrochemical measurements

All the electrochemical tests were conducted in coin cells (CR2032). The working electrode was prepared by spreading the mixed slurry of active material and PVDF binder in N-methyl-2-pyrrolidone (NMP) solvent with a weight ratio of 9.5:0.5 onto Cu foil , and then dried at 100°C in vacuum for 10 hours. The loading mass of hard carbon electrode was controlled between 1.5 ~ 2.5 mg cm^{-2}. The electrolyte was a solution of 1 M $NaClO_4$ in ethylene (EC) and diethyl carbonate (DEC) (1:1 in volume). A sodium foil was used as the counter electrode and glass fiber was used as the separator. All the operations were operated in the argon-filled glove box. The discharge and charge tests were carried out on a Land BT2000 battery test system (Wuhan, China) in a voltage range of 0–3 V at various C-rates under room temperature. A sodium-ion full cell was constructed using HCS1600 as the negative electrode and $Na_{2/3}Ni_{1/3}Mn_{2/3}O_2$ as the positive electrode in a CR2032 coin-type cell. Synthesis method of the $Na_{2/3}Ni_{1/3}Mn_{2/3}O_2$ material was reported before.[43] The weight ratio of the two electrodes (negative/positive) was 1:4. The full cells were charged and discharged in a voltage range of 0–3.9 V at 0.1C current rate.

Results and discussion

Structural and morphological characterizations

Figure 1a shows the SEM image of the typical morphology of HCS. HCS has

perfect spherical shape and a uniform particle size, and the surfaces are very smooth. The diameter of the obtained carbon spherules is about 1 μm. The size of HCS is mainly determined by the dewatering procedure at low temperatures rather than the following carbonization process, thus HCS carbonized at different temperature has the same size.

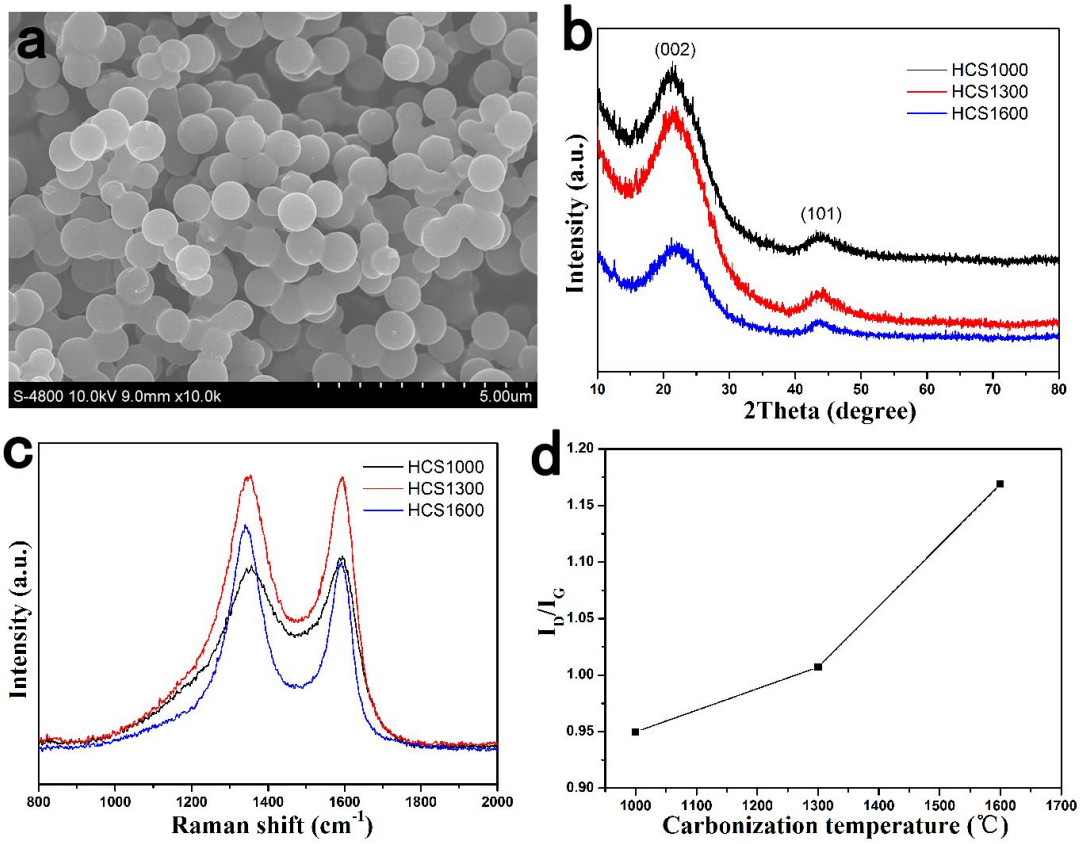

Figure 1. The structure of HCS carbonized at different temperature. (a) SEM image; (b) XRD patterns; (c) Raman spectra; (d) The relation curve of I_D/I_G and carbonization temperature.

The structure of HCS with different carbonized temperatures was investigated by XRD and Raman spectroscopy, and the results are shown in Figure 1b and Figure 1c. All XRD patterns show the broad peaks of (002) and (101), which confirm their amorphous structure. Raman spectra exhibit two broad bands of D-band peak at ~1343 cm^{-1} (the defect-induced band) and G-band peak at ~1589 cm^{-1} (the crystalline graphite band).[41] As shown in Figure 1d, the intensity of I_D/I_G ratios are 0.950, 1.007 and 1.169 for HCS carbonized at 1000°C (HCS1000), 1300°C (HCS1300) and 1600°C (HCS1600) respectively, increasing with the increase of carbonization temperature. It indicates that the disorder degree increases with the increase of carbonized temperature,[42] which is contrary to people's common sense. The mechanism is still not clear at the moment.

Brunauer-Emmett-Teller (BET) measurement was used to investigate specific surface area of HCS1000 before and after coating soft carbon, as shown in Figure S1. The result shows a much larger specific surface area for HCS1000 sample without coating, while the coated HCS1000 sample only has a small surface area. This

illustrates that coating soft carbon can effectively reduce the exposed surface area.

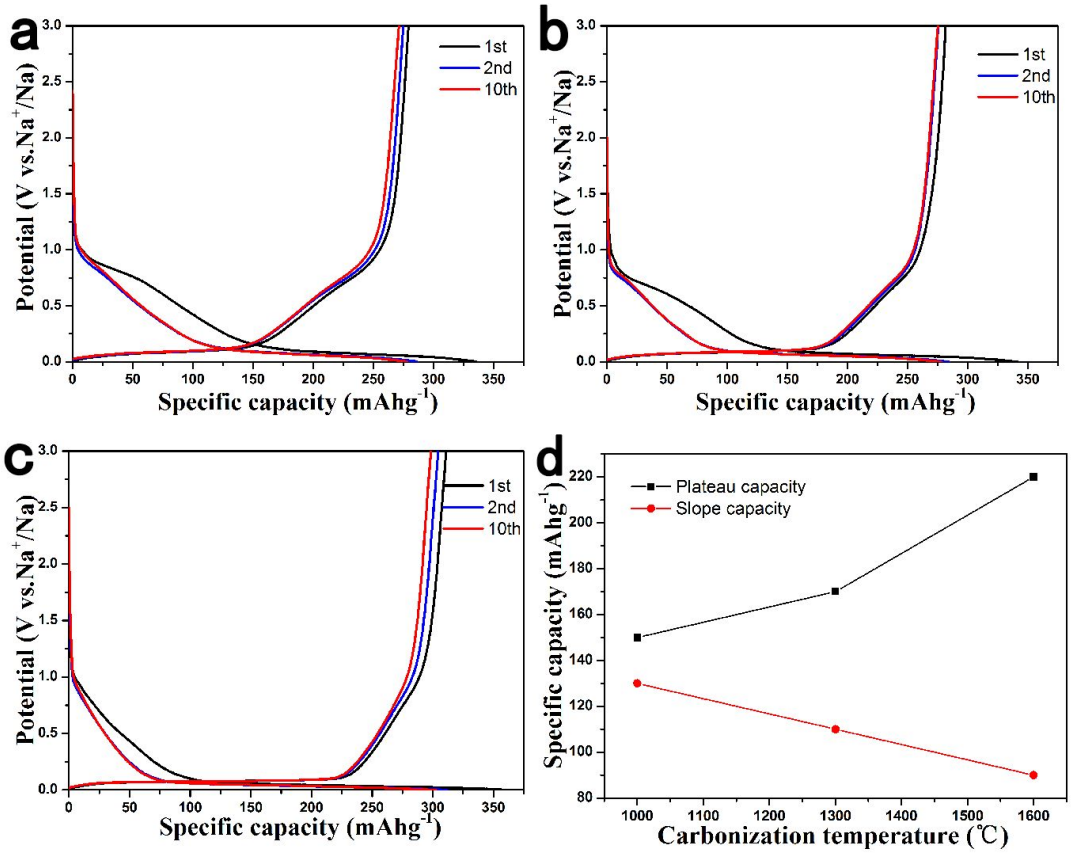

Figure 2. Discharge and charge curves for the 1st, 2nd and 10th cycles of (a) HCS1000, (b) HCS1300 and (c) HCS1600; (d) The relation curves of the plateau and slope capacity and carbonization temperature.

Electrochemical performances of HCS

The electrochemical performance of HCS was first evaluated in half cells with Na as the counter electrode， as shown in Figure 2. Figure 2a shows the 1st, 2nd and 10th discharge/charge profiles of the HCS1000 electrode at 0.1C (30 mA g^{-1}). The initial discharge and charge capacities are 335 mAh g^{-1} and 279 mAh g^{-1}, respectively. The profile can be divided into two regions of a slope above 0.2 V and a plateau close to 0 V. The charge capacity of the plateau region is 150 mAh g^{-1}, about 53% of the total capacity. The initial Coulombic efficiency is 83%, while the initial Coulombic efficiency of the HCS1000 sample without coating soft carbon only is 54% (Fig. S2). The high initial Coulombic efficiency is attributed to the soft carbon coated on the surface of HCS from the pyrolysis of toluene, which significantly reduces the contact area with electrolyte and the formation of solid electrolyte interphase (SEI). Meantime, the polarization between discharge and charge is also reduced, the plateau capacity can completely be utilized above 0 V. Therefore, the coated HCS1000 sample has higher capacity than the sample without coating. After the tenth cycles, the Coulombic efficiency rises to 99%, it suggests that coating is an effective way to improve Coulombic efficiency and reduce polarization of hard carbon.

Figure 2b and Figure 2c show the 1st, 2nd and 10th discharge/charge profiles of

HCS1300 and HCS1600 electrodes, respectively. Compared with HCS1000 electrode, the carbonized temperature mainly affects the percentage of the plateau region among the charge capacity, while has little influence on Coulombic efficiency. The plateau capacity of HCS1300 is 170 mAh g^{-1}, about 60% of the total capacity. For HCS1600, the plateau capacity increases to 220 mAh g^{-1}, accounting to 70% of the whole capacity. As shown in Figure 2d, the percentage of the plateau capacity increases with carbonized temperature whereas the slopping capacity decreases. Since the plateau at the low potential region may correspond to Na adsorption/desorption in the nanopores of carbon particles,[44-47] it indicates that the quantity of nanopores increases with the increase of carbonized temperature.

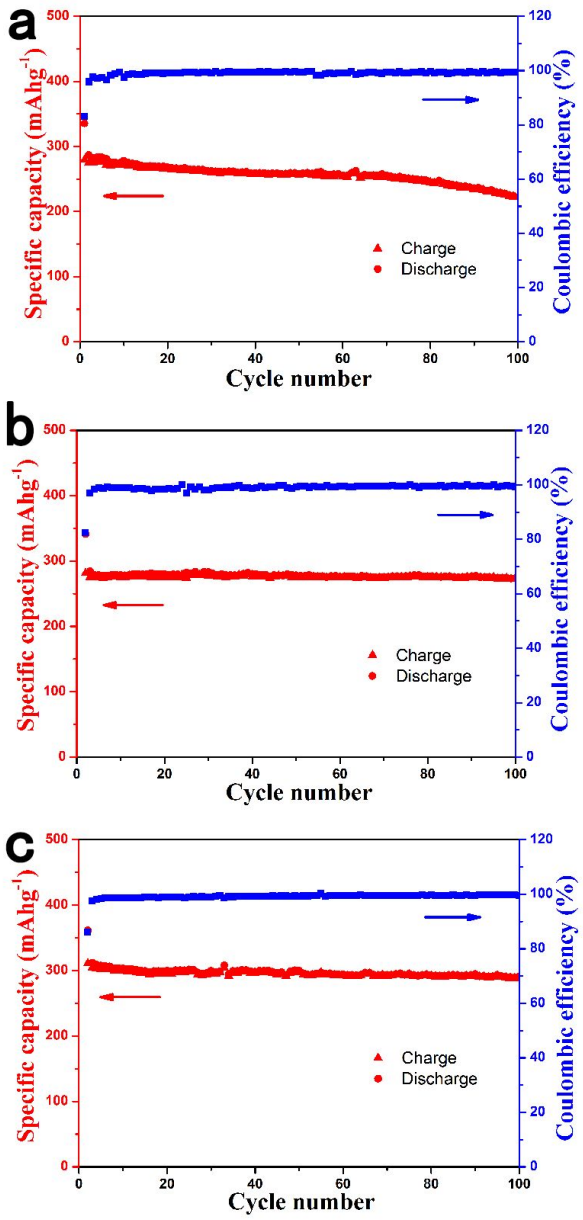

Figure 3. Cycling performance of (a) HCS1000, (b) HCS1300 and (c) HCS1600.

Figure 3 shows the cycling performance of HCS1000, HCS1300 and HCS1600 electrodes at 0.1C for 100 cycles. After 100 cycles, the HCS1000 sample retains a capacity of 222 mAh g^{-1}, corresponding to a capacity retention of 80%. However, the HCS1300 and the HCS1600 exhibit much lower capacity decay, about 272 mAh g^{-1} and 290 mAh g^{-1} are remained after 100 cycles respectively, corresponding to capacity retention of 97% and 93%.

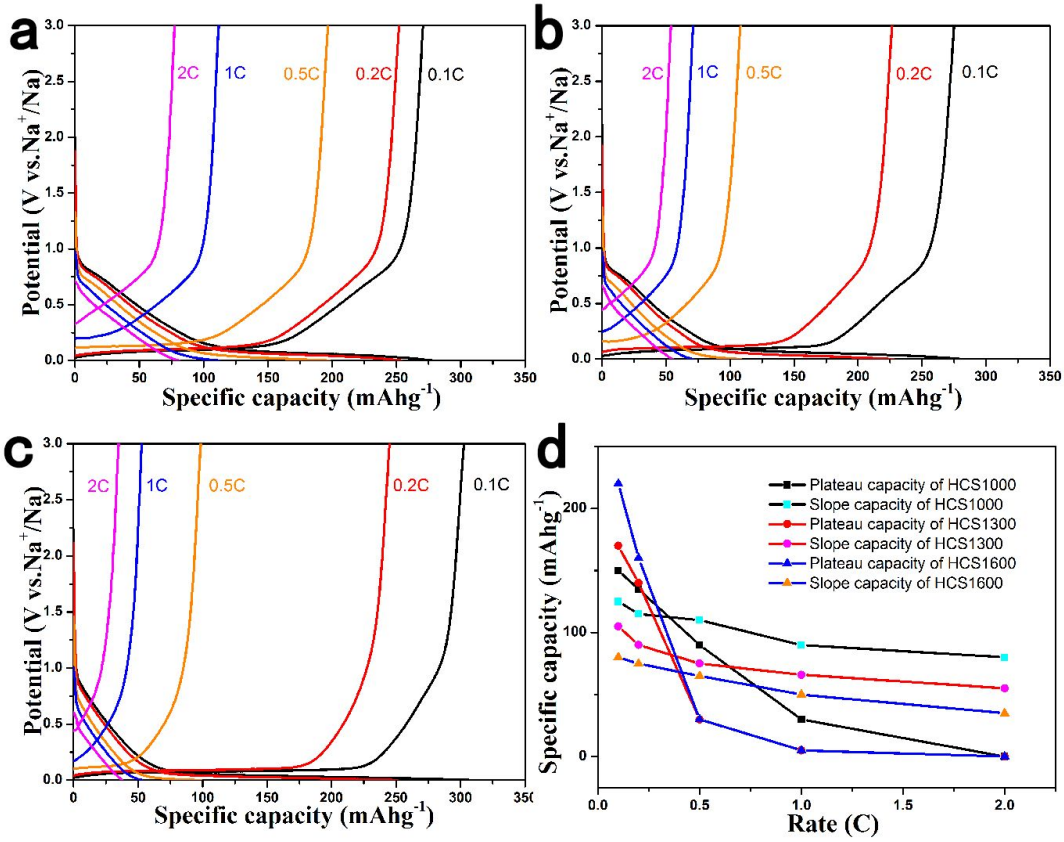

Figure 4. Rate performance of (a) HCS1000, (b) HCS1300 and (c) HCS1600 samples; (d) The retained capacity from plateau and slope contributions under different current rates.

The rate performance of HCS electrodes is shown in Figure 4. The cells were discharged and charged at various rates from 0.1C to 2C for five cycles. The HCS1000 sample delivers a specific capacity of 201 mAh g^{-1} at 0.5C, but HCS1300 and HCS1600 only deliver a specific capacity of 110 mAh g^{-1} and 98 mAh g^{-1} at 0.5C. When the current rate is reduced, the capacity can return to the previous value, suggesting a good stability of HCS under a wide current range. Overall, the HCS shows poor rate capability as other hard carbon materials reported before, and the rate performance deteriorates with the rise of carbonized temperature (Fig. S3). It is interesting to find that the total capacity decay at high rate is mainly due to the rapid plateau capacity decay as shown in Figure 4d. This suggests that Na adsorption/desorption in the nanopores at the low potential plateau region has the worse kinetic property than Na adsorption/desorption between the graphene layers at the slope region. In order to check whether the insertion step or extraction step limits

the rate performance, we performed the asymmetric current rate test. The HCS1600 electrode was discharged (Na insertion) at a constant current rate of 0.1C and charged (Na extraction) at different rates. The results are shown in Figure 5. It can be seen that even at a very high charging rate of 20C (3 min charge), the reversible charge capacity of 270 mAh g^{-1} is achieved. This result indicates that Na extraction from hard carbon is very fast and Na insertion into hard carbon is the limited step.

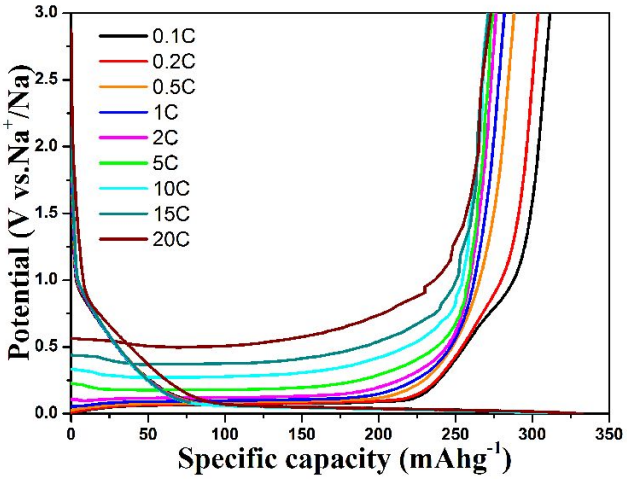

Figure 5. Rate performance of the HCS1600 electrode discharged at the same current rate of 0.1C.

Full cell performance of sodium-ion batteries

To test the actual performance of HCS in full cells, we select the air-stable P2-$Na_{2/3}Ni_{1/3}Mn_{2/3}O_2$ material as the positive electrode to assemble a full cell. P2-$Na_{2/3}Ni_{1/3}Mn_{2/3}O_2$ cathode material is of particular interest because of the high operation with $Ni^{2+}/Ni^{3+}/Ni^{4+}$ redox couple and stability in cycling.[43] Unlike other layered oxides, this material is very stable in air and even in water as shown in Figure S4. Herein, we tested the electrochemical performance of the $Na_{2/3}Ni_{1/3}Mn_{2/3}O_2$ electrode in the voltage range of 2.5-3.9 V to avoid the P2-O2 phase transition. The stable cycle performance is achieved with a reversible capacity of 80 mAh g^{-1} in a Na/$Na_{2/3}Ni_{1/3}Mn_{2/3}O_2$ half cell (Fig. S5).

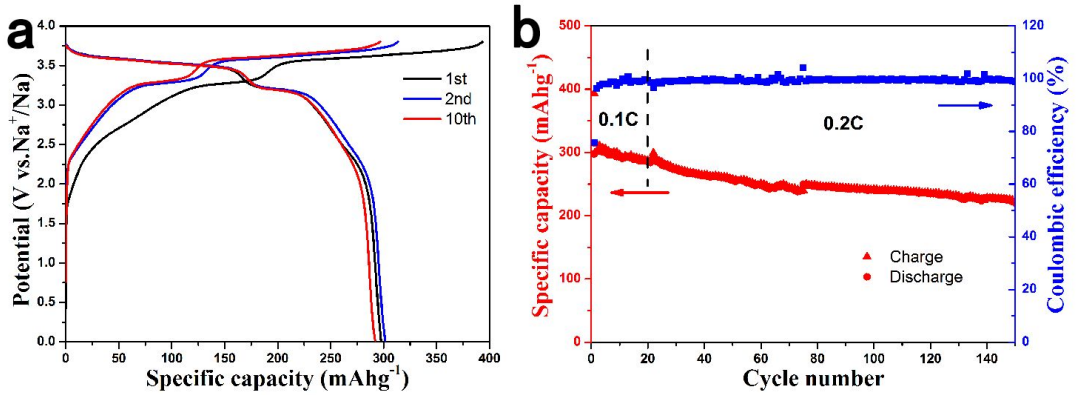

Figure 6. The performance of a coin-type HCS1600/$Na_{2/3}Ni_{1/3}Mn_{2/3}O_2$ full cell. (a) Charge and discharge curves for the 1st, 2nd and 10th cycles and (b) cycling performance.

We fabricated the coin-type full sodium-ion batteries with the $Na_{2/3}Ni_{1/3}Mn_{2/3}O_2$ positive electrode and the HCS1600 negative electrode. The cell was cycled at 0.1C for the first 20 cycles, then at 0.2C for the subsequent cycles. Figure 6a shows the charge and discharge curves of a $Na_{2/3}Ni_{1/3}Mn_{2/3}O_2$/HCS1600 cell at room temperature. It can be seen that the $Na_{2/3}Ni_{1/3}Mn_{2/3}O_2$/HCS1600 full cell exhibits a high average operating voltage of 3.5 V, a high capacity more than 300 mAh g^{-1} (based on negative electrode) and a high initial Coulombic efficiency of 76%. The theoretical energy density of this system is estimated to be 200 Wh/kg owing to the low average storage voltage of HCS1600. The $Na_{2/3}Ni_{1/3}Mn_{2/3}O_2$/HCS1600 full cell also exhibits superior cycle performance as shown in Figure 6b with a capacity retention of 73% after 150 cycles. To the best of our knowledge, this is the first report to demonstrate a sodium-ion full cell with a relatively high operating voltage and long cycling performance. These desired promising properties are believed to be close to the level of practical application.

Conclusions

In summary, we fabricated monodispersed hard carbon spherules coated by soft carbon, and found that coating can significantly improve the initial Coulombic efficiency from 54% to 83%. Next, we investigated the influence of carbonized temperature on micro-structure and electrochemistry performance of HCS in detail for the first time. It is interesting to find that the plateau capacity at the low potential region increases with the increase of carbonization temperature. When the carbonization temperature is increased from 1000°C to 1600°C, the plateau capacities increase from 150 mAh g^{-1} to 220 mAh g^{-1} at 0.1C. HCS also displays excellent cycling performance with capacity retention of 93% of HCS1600 after 100 cycles. The rate performance of HCS is limited by the Na insertion process. When the HCS1600 electrode was discharged at a low current rate, the charging rate can be up to 20C, a reversible capacity of 270 mAh g^{-1} is achieved. Finally, the application of HCS was also demonstrated in full cells with air-stable P2-$Na_{2/3}Ni_{1/3}Mn_{2/3}O_2$ positive electrode. The full cell exhibits a high average operating voltage of 3.5 V, a high capacity more than 300 mAh g^{-1}, a high initial Coulombic efficiency of 76% and superior cycling performance. These outstanding performances make this system be closer to the practical application.

Acknowledgements

This work was supported by funding from the NSFC (51222210, 11234013), “973” Projects (2010CB833102, 2012CB932900), and One Hundred Talent Project of the Chinese Academy of Sciences.

Notes and references

1 M. Armand and J. M. Tarascon, *Nature,* 2008, **451**, 652–657.

2 L. M. Suo, Y. -S. Hu, H. Li, M. Armand and L. Q. Chen, *Nat. Commun.,* 2013, **4**, 1481.

3 H. L. Pan, Y. -S. Hu and L. Q. Chen, *Energy Environ. Sci.,* 2013, **6**, 2338–2360.

4 J. M. Tarascon, *Nature Chemistry,* 2010, **2**, 510.

5 S. W. Kim, D. H. Seo, X. Ma, G. Ceder and K. Kang, *Adv. Energy Mater.,* 2012, **2**, 710–721.

6 M. D. Slater, D. Kim, E. Lee and C. S. Johnson, *Adv. Funct. Mater.,* 2013, **23**, 947–958.

7 V. Palomares, M. C. Cabanas, E. C. Mart´ınez, M. H. Hanb and T. Rojo, *Energy Environ. Sci.,* 2012, **5**, 5884–5901.

8 M. D. Slater, D. Kim, E. Lee and C. S. Johnson, *Adv. Funct. Mater.,* 2013, **23**, 947–958.

9 N. Yabuuchi, M. Kajiyama, J. Iwatate, H. Nishikawa, S. Hitomi, R. Okuyama, R. Usui, Y. Yamada and S. Komaba, *Nat. Mater.,* 2012, **11**, 512–517.

10 M. Sathiya, K. Hemalatha, K. Ramesha, J. M. Tarascon and A. S. Prakash, *Chem. Mater.,* 2012, **24**, 1846–1853.

11 Z. L. Jian, L. Zhao, H. L. Pan, Y. -S. Hu, H. Li, W. Chen and L. Q. Chen, *Electrochem. Commun.,* 2012, **14**, 86–89.

12 H. Wang, S. Yuan, D. Ma, X. Huang, F. Meng and X. Zhang, *Adv. Energy Mater.,* 2014, **4**, 1301651.

13 H. Yoshida, N. Yabuuchi, K. Kubota, I. Ikeuchi, A. Garsuch, M. S. Dobrick and S. Komaba, *Chem. Commun.,* 2014, **50**, 3677–3680.

14 S. Y. Xu, X. Y. Wu, Y. M. Li, Y. -S. Hu and L. Q. Chen, *Chin. Phys. B*, 2014, **23**, 118202.

15 P. Ge and M. Fouletier, *Solid State Ionics,* 1988, **28**, 1172–1175.

16 M. M. Doeff, Y. P. Ma, S. J. Visco and L. C. Dejonghe, *J. Electrochem. Soc.,* 1993, **140**, L169–L170.

17 J. Zhao, L. W. Zhao, K. Chihara, S. Okada, J. Yamaki, S. Matsumoto, S. Kuze and K. Nakane, *J. Power Sources,* 2013, **244**, 752–757.

18 J. F. Qian, Y. Chen, L. Wu, Y. L. Cao, X. P. Ai and H. X. Yang, *Chem. Commun.,* 2012, **48**, 7070–7072.

19 Y. H. Xu, Y. J. Zhu, Y. H. Liu and C. S. Wang, *Adv. Energy Mater.,* 2013, **3**, 128–133.

20 L. F. Xiao, Y. L. Cao, J. Xiao, W. Wang, L. Kovarik, Z. M. Nie and J. Liu, *Chem. Commun.,* 2012, **48**, 3321–3323.

21 V. L. Chevrier and G. Ceder, *J. Electrochem. Soc.,* 2011, **15**, A1011–A1014.

22 H. L. Pan, X. Lu, X. Q. Yu, Y. -S. Hu, H. Li, X. Q. Yang and L. Q. Chen, *Adv. Energy Mater.,* 2013, **3**, 1186–1194.

23 L. Zhao, H. L. Pan, Y. -S. Hu, H. Li and L. Q. Chen, *Chin. Phys. B,* 2012, **21**, 028201.

24 Y. Sun, L. Zhao, H. L. Pan, X. Lu, L. Gu, Y. -S. Hu, H. Li, M. Armand, Y. Ikuhara,

L. Q. Chen and X. J. Huang, *Nat. Commun*., 2013, **4**, 1870.
25 Y. S. Wang, X. Q. Yu, S. Y. Xu, J. M. Bai, R. J. Xiao, Y. -S. Hu, H. Li, X. Q. Yang, L. Q. Chen and X. J. Huang, *Nat. Commun.,* 2013, **4**, 2365.
26 L. Zhao, J. M. Zhao, Y. -S. Hu, H. Li, Z. B. Zhou, M. Armand and L. Q. Chen, *Adv. Energy Mater.,* 2012, **2**, 962–965.
27 Y. Park, D. S. Shin, S. H. Woo, N. S. Choi, K. H. Shin, S. M. Oh, K. T. Lee and S. Y. Hong, *Adv. Mater.,* 2012, **24**, 3562–3567.
28 Y. Wen, K. He, Y. J. Zhu, F. D. Han, Y. H. Xu, I. Matsuda, Y. Ishii, J. Cumings and C. S. Wang, *Nat. Commun.,* 2014, **5**, 4033.
29 P. Thomas and D. Billaud, *Electrochim. Acta.,* 2002, **47**, 3303–3307.
30 A. Ponrouch, E. Marchante, M. Courty, J. M. Tarascon and M. RosaPalac´ın, *Energy Environ. Sci.,* 2012, **5**, 8572–8583.
31 J. Zhao, L. Zhao, K. Chihara, S. Okada, J. Yamaki, S. Matsumoto, S. Kuze and K. Nakane, *J. Power Sources,* 2013, **244**, 752–757.
32 D. A. Stevens and J. R. Dahn, *J. Electrochem. Soc.,* 2000, **147**, 1271–1273.
33 S. Komaba, W. Murata, T. Ishikawa, N. Yabuuchi, T. Ozeki, T. Nakayama, A. Ogata, K. Gotoh and K. Fujiwara, *Adv. Funct. Mater.,* 2011, **21**, 3859–3867.
34 S. Wenzel, T. Hara, J. Janek and P. Adelhelm, *Energy Environ. Sci.,* 2011, **4**, 3342–3345.
35 K. Tang, L. J. Fu, R. J. White, L. H. Yu, M. M. Titirici, M. Antonietti and J. Maier, *Adv. Energy Mater.,* 2012, **2**, 873–877.
36 Y. L. Cao, L. F. Xiao, M. L. Sushko, W. Wang, B. Schwenzer, J. Xiao, Z. M. Nie, L. V. Saraf, Z. G. Yang and J. Liu, *Nano. Lett.,* 2012, **12**, 3783–3787.
37 H. G. Wang, Z. Wu, F. I. Meng, D. l. Ma, X. l. Huang, L. M. Wang and X. B. Zhang, *ChemSusChem,* 2013, **6**, 56–60.
38 Q. Wang, H. Li, L. Q. Chen and X. J. Huang, *Carbon*, 2001, **39**, 2211–2214.
39 M. M. Titirici, M. Antonietti and N. Baccile, *Green Chem*., 2008, **10**, 1204-1212.
40 B. Hu, K. Wang, L. Wu, S. H. Yu, M. Antonietti and M. M. Titirici, *Adv. Mater.,* 2010*,* **22***,* 813 – 828.
41 L. Qie, W. M. Chen, H. H. Xu, X. Q. Xiong, Y. Jiang, F. Zou, X. L.Hu, Y. Xin, Z. L. Zhang and Y. H. Huang, *Energy Environ. Sci.,* 2013, **6**, 2497–2505.
42 M. M. Doeff, Y. Hu, F. M. Larnon and R. Kostecki, *Electrochem. Solid St.,* 2003, **6**, A207–A209.
43 Z. H. Lu and J. R. Dahn, *J. Electrochem. Soc.,* 2001, **148**, A1225–A1229.
44 A. Mabuchi, K. Tokumitsu, H. Fujimoto and T. Kasuh, *J. Electrochem. Soc.,* 1995, **142**, 1041–1046.
45 D. A. Stevens and J. R. Dahn, *J. Electrochem. Soc*., 2000, **147**, 4428–4431.
46 S. M. Mamun, M. Herstedt, K. Oikawa, T. Gustafsson, T. Otomo, M. Furusaka, T. Kamiyama, H. Sakaebe and K. Edstrom, *Appl. Phys. A: Mater. Sci. Process,* 2002, **74**, S1028–1030.
47 S. Komaba, W. Murata, T. Ishikawa, N. Yabuuchi, T. Ozeki, T. Nakayama, A. Ogata, K. Gotoh and K. Fujiwara, *Adv. Funct. Mater.,* 2011, **21**, 3859–3867.